PRECIPITATION IN ALLOY 718:

A COMBINED AEM AND APFIM INVESTIGATION

M.G. Burke and M.K. Miller*

Westinghouse Science and Technology Center
Pittsburgh, PA 15235

**Metals and Ceramics Division*
Oak Ridge National Laboratory
Oak Ridge, TN 37831-6376

Abstract

The desirable mechanical properties of nickel-base superalloy Alloy 718 are associated with a complex multiphase microstructure that is produced by a multistage heat treatment. In this investigation, the primary matrix strengthening phases (γ'' and γ') and grain boundary phases (δ and Laves) formed during various aging treatments have been characterized by a combination of analytical electron microscopy and atom probe field ion microscopy. Detailed structural and chemical analyses have been performed to identify the phases and provide information concerning the precipitation sequence for the primary γ'' and δ phases. The results of this investigation have revealed that there is a wide variation in the composition of the phases and that their compositions are affected by the thermal treatment and location within the complex microstructure.

Superalloys 718, 625 and Various Derivatives
Edited by Edward A. Loria
The Minerals, Metals & Materials Society, 1991

INTRODUCTION

Alloy 718, a Nb-modified nickel-base superalloy widely used in gas turbine and related applications, derives its good mechanical properties and structural stability at elevated temperatures (~650°C) from a complex microstructure which is produced by a multistage heat treatment.[1,2] The primary strengthening phases in Alloy 718 are a DO_{22}-ordered γ'' phase and an $L1_2$-ordered γ' phase. The γ' and γ'' phases are coherent with the face centered cubic γ matrix. The compositions of both these phases have been described as Ni_3(Nb, Al, Ti) with varying amounts of Nb, Al and Ti. However, the fine size of these precipitates makes the measurement of their compositions experimentally difficult by conventional analytical techniques. A number of other phases such as δ (Ni_3Nb), Laves, and MC-type carbides have also been observed.[2]

In this study, the techniques of analytical electron microscopy (AEM) and atom probe field ion microscopy (APFIM) have been used to fully characterize the precipitate phases and to determine the composition of the γ matrix following a multistage heat treatment.

ANALYTICAL TECHNIQUES

The AEM has the ability to determine the crystal structure from electron diffraction patterns and determine the composition with an energy dispersive x-ray spectrometer (EDS). In addition, the AEM has a relatively large field of view enabling the detection and characterization of low volume fraction or low number density features and permits the determination of variations in the distribution of phases. This ability is particularly important in Alloy 718 since some of the precipitates form preferentially along grain and other internal boundaries. With its near-atomic spatial resolution and its ability to analyze all elements simultaneously, the APFIM is well suited to characterize the finer precipitates and the matrix in these complex alloys.[3,4] The combination of these two analytical techniques permit the microstructure to be fully characterized.[5-7]

The atom probe is a combination of a field ion microscope and a mass spectrometer, as shown in Fig. 1. The field ion microscope is used to obtain highly magnified (~10^6X) images of the specimen. The mass spectrometer is used to analyze features selected from that field ion image. A schematic diagram of a field ion microscope is shown in Fig. 2. After cooling to cryogenic temperatures, the field ion image of the specimen surface is obtained by first introducing approximately 10^{-3} Pa of image gas into the ultrahigh vacuum chamber and then applying a positive voltage to the specimen. At a certain voltage, dependent on the sharpness of the needle-shaped specimen and the image gas used, the field ion image will appear on the channel plate and phosphor screen assembly placed 50 mm in front of the specimen. The principle of field ion microscopy is shown in Fig. 2. The image gas atoms that are near the positively-charged specimen are polarized and then attracted to the specimen. The image gas atoms are then thermally accommodated to the cryogenic temperature. If the field is sufficient, the image gas atom may then be ionized and radially projected away from the surface toward the fluorescent screen where the field ion image is formed. An example of a field ion image of Alloy 718 is shown in Fig. 3. The brightly-imaging regions are the γ'' and γ' precipitates and the darker regions are the γ matrix. In Alloy 718 since the γ'' and γ' precipitates exhibit similar contrast, the identification of the precipitate type is made from the size, morphology, and composition determined in the mass spectrometer.[5] A chemical analysis of a specific

region, such as a precipitate, is made by rotating the specimen until the image of that feature falls over the aperture in the channel plate and screen assembly. The aperture is the central portion of the dark disc in the center of the field ion image shown in Fig. 3, and serves as the entrance to the mass spectrometer. The surface atoms of the specimen may then be removed from the specimen by increasing the voltage on the specimen. This is done in practice by the superposition of a high voltage pulse onto the standing voltage on the specimen. Although ionized atoms are removed from the entire specimen, only those whose trajectories pass through the aperture are analyzed in the time-of-flight mass spectrometer. The mass-to-charge ratio of those ions, m/n, is given by equating the potential energy of the atom on the specimen surface under the electric field, E, to the kinetic energy that is acquired on leaving the surface :

$$\frac{m}{n} = 0.193\ E\ \frac{t^2}{d^2}$$

where d is the distance traveled from the specimen to the single atom detector at the end of the mass spectrometer, and t is the flight time of the ion over that distance. Modern analytical atom probes incorporate an energy-compensating lens into the mass spectrometer to improve the mass resolution. The composition of a small volume of material is determined by removing a statistically significant number of atoms from the specimen and counting the number of atoms of each element compared to the total number of atoms collected in that volume. A more complete description of the atom probe may be found elsewhere.[3]

EXPERIMENTAL

Material

The nominal composition of the material used in this investigation is given in Table I. In addition to the elements listed in this table, trace amounts of 0.02 at. % P, 0.03% B, 0.05% Cu and 0.002% S were also present.

TABLE I. NOMINAL COMPOSITION OF ALLOY 718

Nb	Al	Ti	Fe	Cr	Co	Mo	Mn	Si	C	Ni	
5.2	0.43	0.95	19.6	19.4	0.26	3.0	0.16	0.21	0.05	bal.	wt%
3.2	0.95	1.15	20.3	20.3	0.26	1.81	0.17	0.43	0.26	bal.	at%

Heat Treatment

The multistage heat treatments that were used in this study are listed in Table II. The material was fast air-cooled to room temperature between each stage. Both AEM and APFIM specimens were prepared from bulk material by conventional electropolishing techniques.

TABLE II. HEAT TREATMENTS

Code	Stages			
AB	1h 1038°C	8h 982°C		
ABDE	1h 1038°C	8h 982°C	8h 760°C	8h 650°C
AC	1h 1038°C	8h 870°C		
ACD	1h 1038°C	8h 870°C	8h 760°C	
ACDE	1h 1038°C	8h 870°C	8h 760°C	8h 650°C
AD	1h 1038°C	8h 760°C		

Instrumentation

AEM was performed with a Phillips EM400T analytical electron microscope equipped with a Link Analytical windowless LZ-5 energy dispersive x-ray spectrometer (EDS) and AN10/85S analyzer. The phases present in the microstructure were identified by electron diffraction techniques and EDS quantitative microanalysis.

The APFIM characterization was performed in the Oak Ridge National Laboratory energy-compensated atom probe.[8] The mass resolution of this instrument is sufficient to fully resolve the isotopes of all elements present in Alloy 718. Common isobar overlaps were deconvoluted by standard techniques. Field ion micrographs were obtained with neon as the image gas. The specimen temperature used to obtain the field ion images and for atom probe microanalysis was 50K. All compositions in this paper are quoted in atomic percent.

MICROSTRUCTURE

Laves Precipitates

Coarse blocky precipitates, as shown in Fig. 4, were observed primarily along grain boundaries in all thermally annealed specimens. These precipitates were identified by electron diffraction as the ordered Laves phase with a C14 crystal structure. The lattice parameters was determined to be $a_o \simeq 0.47$ nm and $c_o \simeq 0.75$ nm. The composition of this phase as measured by EDS microanalysis is shown in Table III. This composition is consistent with $(Ni_{0.5}Fe_{0.25}Cr_{0.25})_2(NbMoSi)$. The size, morphology and presence of this precipitate in all heat treatments indicated that this phase formed either during the solidification process or during the anneal at 1038°C. Its presence after the 1038°C annealing stage also indicated that this temperature was not sufficient to produce a precipitate free starting condition.

MC carbides

Another type of coarse precipitate was observed in all heat treatments as shown in Fig. 5. These blocky carbides were approximately 0.5 μm in size. Electron diffraction revealed

that these precipitates were MC-type carbides. The metal content of one of these precipitates is given in Table III and indicated that these precipitates are titanium-rich (TiNb)C. EDS analysis indicated that the matrix near these precipitates was depleted in Ti. Similar to the Laves phase, it appears that these carbides were also formed either during the solidification process or during the 1038°C anneal.

δ Precipitates

Aging at 870°C produced precipitates with needle-like (~1 to 8 μm) and globular (~1 μm) morphologies, as shown in Fig. 6. This phase was observed primarily at grain boundaries although some intragranular precipitates were also observed. These precipitates were characterized by a highly faulted internal structure, as shown in Fig. 7. The orthorhombic DO_a-ordered crystal structure determined from electron diffraction indicated that these precipitates were δ phase. The composition of this phase as measured by EDS is given in Table III. The composition of these precipitates was enriched in Nb and Ti and depleted in Fe and Cr compared to the matrix composition. EDS microanalysis of the γ matrix surrounding these δ precipitates indicated a local depletion of Nb of up to 50%.

Primary γ″ Precipitates

Aging at 870°C also produced a widespread distribution both throughout the matrix and also at some coherent twin boundaries of coarse lenticular precipitates ~0.3 μm in length, as shown in Fig. 8. The DO_{22}-ordered crystal structure determined from electron diffraction indicated that these precipitates were γ″. The composition of these precipitates was measured by both EDS and APFIM and are also included in Table III. These precipitates were found to be enriched in Nb and Ti and depleted in Al, Fe, Cr and Mo compared to the γ matrix. A comparison of the EDS and APFIM results show good agreement between the two analytical techniques. These coarse precipitates will be referred to as primary γ″.

Zones free of these primary γ″ precipitates were observed surrounding the δ precipitates. These denuded zones are also an indication of the Nb depletion adjacent to the δ precipitates. The presence of these γ″-free zones also suggests that the γ″ forms after the δ precipitates.

TABLE III. AVERAGE COMPOSITIONS OF THE COARSE PRECIPITATES
* denotes APFIM analysis, all others EDS. The balance of these analyses is nickel.

Heat Treatment	Phase	Nb	Al	Ti	Fe	Cr	Co	Mo	Mn	Si
	Laves	18.8	0.1	0.6	15.0	15.3	-	10.2	0.05	4.5
	MC	14.6	0.1	80.0	0.9	1.9	-	0.5	-	1.9
AC	δ	20.4	0.8	3.0	5.3	3.4	-	2.2	0.4	0.1
AC	γ″	21.3	0.8	4.0	3.3	2.49	-	0.4	0.1	-
AC*	γ″	23.8	0.6	6.3	2.2	1.5	0.1	0.7	0.04	0.1
ACDE*	γ″	22.4	0.5	5.6	1.1	0.7	0.3	1.1	0.42	0.1

Secondary γ″ Precipitates

In specimens that had been aged at 760°C, some fine γ″ precipitates were also observed, as shown in Fig. 9. These precipitates were lenticular in shape and between 10 and 40 nm in extent. In the absence of δ or primary γ″, these precipitates were observed throughout the matrix and at grain boundaries. However, zones denuded in these precipitates extended approximately 0.4 μm from the δ precipitates. These smaller precipitates will be referred to as secondary γ″. The secondary γ″ precipitates were observed in the materials that had been subjected to heat treatments ABDE, ACD, ACDE, and AD, i.e. independent of whether the 870°C stage was used. The compositions of these γ″ precipitates were found to depend on the heat treatment and the position in relationship to the primary γ″, as shown in Table IV. In heat treatments that did not produce primary γ″ (i.e. ABDE and AD), the Nb composition of the secondary γ″ was similar to the primary γ″ in other heat treatments. In materials that contained primary γ″ (i.e ACD and ACDE), the secondary γ″ that was removed from the primary γ″ was significantly higher in Nb and lower in Al than that of the secondary γ″ in the vicinity of the primary γ″. However, no secondary γ″ was observed within 25 nm of the primary γ″. A wide variation in the ratio of Nb to Nb+Al+Ti was also observed in heat treatment ACDE.

TABLE IV. AVERAGE COMPOSITION OF SECONDARY γ″ PRECIPITATES
The balance of these APFIM analyses is nickel.
* in the vicinity of primary γ″ precipitates

Heat Treatment	Nb	Al	Ti	Fe	Cr	Co	Mo	Mn	Si
ABDE	23.1	1.27	5.41	1.91	1.53	0.08	0.89	0.05	0.13
ACD	24.5	1.18	5.99	1.25	0.84	0.20	0.91	0.05	0.07
ACDE	23.0	0.57	4.65	0.73	0.71	0.07	1.36	0.02	0.02
ACDE*	12.0	5.65	8.52	2.27	0.83	0.10	0.26	0.10	0.07
AD	25.1	0.44	4.92	0.86	0.76	0.04	1.05	0.06	0.01

γ′ Precipitates

Another type of precipitate was also evident in material that had been heat treated at 760°C, as shown in Fig. 9. This precipitate was roughly spherical in shape and had a diameter of between 10 and 40 nm. Electron diffraction indicated that this fine precipitate had an $L1_2$-ordered crystal structure and therefore was γ′. The γ′ precipitates were present in a substantially lower number density than the secondary γ″ precipitates. Atom probe analysis revealed that all the fine precipitates within approximately 25 nm of primary γ″ were γ′ and not secondary γ″, Fig. 3. TEM examination also revealed extensive γ′ precipitates within the γ″ denuded zones adjacent to the δ precipitates, as shown in Fig. 10. The compositions of these γ′ precipitates for the heat treatments are given in Table V. The γ′ precipitates were higher in Al and

lower in Nb than the γ'' precipitates. However, all the γ' precipitates were found to contain significant quantities of Nb in addition to Al and Ti.

TABLE V. AVERAGE COMPOSITION OF γ' PRECIPITATES
The balance of these APFIM analyses is nickel.

Heat Treatment	Nb	Al	Ti	Fe	Cr	Co	Mo	Mn	Si
ABDE	10.3	8.09	7.76	2.10	0.86	0.09	0.34	0.18	0.23
ACD	10.4	10.8	7.91	1.81	0.21	0.11	0.18	0.22	0.11
ACDE	8.31	10.2	8.51	1.79	0.41	0.24	0.20	0.22	0.24
AD	10.2	8.00	9.40	2.15	0.50		0.40	0.17	0.35

γ Matrix

The composition of the γ matrix after each stage in the heat treatment was measured in the atom probe. The results of these measurements are shown in Table VI. Also included in Table VI are EDS analyses of the matrix after the AB and AC heat treatments. The EDS results are in good agreement with the atom probe results of the same heat treatment. This composition is more representative of the initial condition of the intragranular regions than the nominal composition of the alloy. A wide variation in the local matrix composition from one position in the microstructure was also evident. The results also indicate that the composition of the matrix changes due to the formation of the various precipitates. In particular, the levels of Nb, Al and Ti decrease as the intermetallic phases precipitate and coarsen. It should also be noted that there is appreciable Nb, Al and Ti remaining in solution after the final heat treatment at 650°C. The levels of Fe, Cr, Mo and Si in the matrix are significantly higher than in the precipitates.

TABLE VI. AVERAGE COMPOSITION OF THE γ MATRIX
* denotes EDS analyses, all others APFIM. The balance of these analyses is nickel.

Heat Treatment	Nb	Al	Ti	Fe	Cr	Co	Mo	Mn	Si
AB	4.57	1.24	1.40	20.1	16.1	0.21	2.43	0.18	0.65
AB*	4.6	1.2	1.2	20.0	21.2	-	2.2	0.2	0.3
ABDE	1.69	0.44	0.34	23.3	21.7	0.24	2.14	0.12	0.63
AC	3.71	1.26	1.21	20.6	15.7	0.24	2.67	0.16	0.68
AC*	3.3	1.3	1.0	19.8	21.1	-	2.2	0.3	0.9
ACD	1.99	0.73	0.59	23.1	18.7	0.18	2.83	0.23	0.61
ACDE	1.69	0.50	0.50	25.5	17.4	0.26	2.32	0.15	0.60
AD	1.97	0.74	0.52	23.8	22.0	0.28	2.41	0.23	0.64

PRECIPITATION SEQUENCE

From these observations, it is possible to construct a sequence of precipitation for the heat treatments studied. The earliest phases to precipitate are the MC-carbide and the Laves phase. These two phases either form during the solidification process or during the 1038°C annealing stage. No significant changes in the microstructure appeared after the 982°C annealing stage. Annealing at 870°C produced the δ and the primary γ'' phases. The δ formed preferentially at grain boundaries and other interfaces such as inclusions and Laves phase whereas the primary γ'' was found nucleated throughout the γ matrix. The zones denuded of primary γ'' surrounding the δ precipitates suggests that the δ precipitates must have formed prior to the primary γ'' precipitates. Annealing at 760°C produced finer secondary γ'' precipitates and γ' precipitates. Again the type of precipitate that was formed was dependent on the proximity of the δ and primary γ'' precipitates. The γ' is formed in the vicinity of these larger Nb-enriched precipitates.

This variation in precipitation behavior with respect to position appears to be a consequence of the variation in the local matrix chemistry. If the local matrix Nb level is too low, the Nb-enriched γ'' will not form. For example, it appears that in regions within 25 nm of the primary γ'' precipitates, the Nb level is too low for secondary γ'' precipitation. However, when or where the niobium content of the matrix is insufficient for the formation of γ'' precipitates it is possible that the superstaturation of solute is still sufficient for γ' precipitates to nucleate. The composition of these precipitates also appears to be influenced by the composition of the matrix at the time of precipitation.

SUMMARY

This combined AEM and APFIM investigation has revealed that the microstructure of Alloy 718 consists of a variety of phases including Laves, MC-carbides, δ, primary and secondary γ'' and γ'. The composition of these phases was found to vary with heat treatment and location within the microstructure. This variation in the compositions of the precipitates and the local inhomogeneities in the matrix makes precise modelling difficult and indicates that a simple model based on a fixed composition for each type of phase is an oversimplication of the actual situation. The results also indicate that there is considerable potential for improving the mechanical properties of this alloy by simpler and less expensive heat treatments.

ACKNOWLEDGMENTS

The authors would like to thank J.J. Haugh of Westinghouse Science and Technology Center, and K.F. Russell of Oak Ridge National Laboratory for their technical assistance, Drs. I.L. Wilson of Westinghouse Electric Corporation and J.L. Nelson of Electric Power Research Institute for helpful discussions and providing the material. This research was sponsored by the Division of Materials Sciences, U.S. Department of Energy, under contract DE-AC05-84OR21400 with Martin Marietta Energy Systems, Inc.

REFERENCES

1. E.E. Brown and D.R. Muzyka, "Nickel-Iron Alloys", Superalloys II, ed. C.T. Sims, N.S. Stoloff and W.C. Hagel, (New York, Wiley and Sons, 1987), 165-188.

2. E.A. Loria, "The Status and Prospects of Alloy 718", *Journal of Metals*, 40 (1988), 36-48.

3. M.K. Miller and G.D.W. Smith, "**Atom Probe Microanalysis: Principles and Applications to Materials Problems**", (Pittsburgh, PA., Materials Research Society, 1989).

4. M.K. Miller, "Ultrahigh-Resolution Chemical Analysis with the Atom Probe", *Internat. Metall. Rev.*, 32(5) (1987), 221-240.

5. M.G. Burke and M.K. Miller, "APFIM/TEM Characterization of Precipitation in Alloy 718", *Journal de Physique*, 50-C8 (1989), 395-400.

6. M.K. Miller and M.G. Burke, "Atom Probe Analysis of the Compositions of γ' and γ'' Intermetallic Phases in Nickel-based Superalloy 718", Proc. Materials Research Society Spring Meeting, San Francisco CA, April 16-21st 1990, in press.

7. M.G. Burke and M.K. Miller, "Grain Boundary Intermetallic Phases in Alloy 718", Proc. Materials Research Society Spring Meeting, San Francisco CA, April 16-21st 1990, in press.

8. M.K. Miller, "The ORNL Atom Probe", *Journal de Physique*, 47-C7 (1986), 493-498.

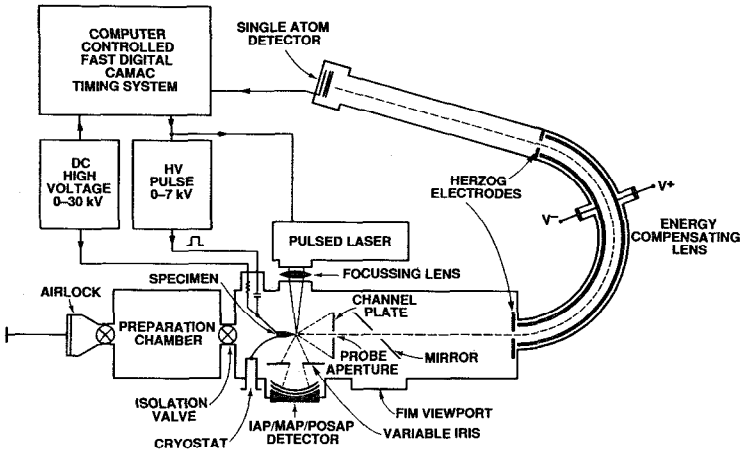

Fig. 1. Schematic diagram of an atom probe. The instrument consists of a field ion microscope and an energy-compensated mass spectrometer. The system is controlled by a microcomputer.

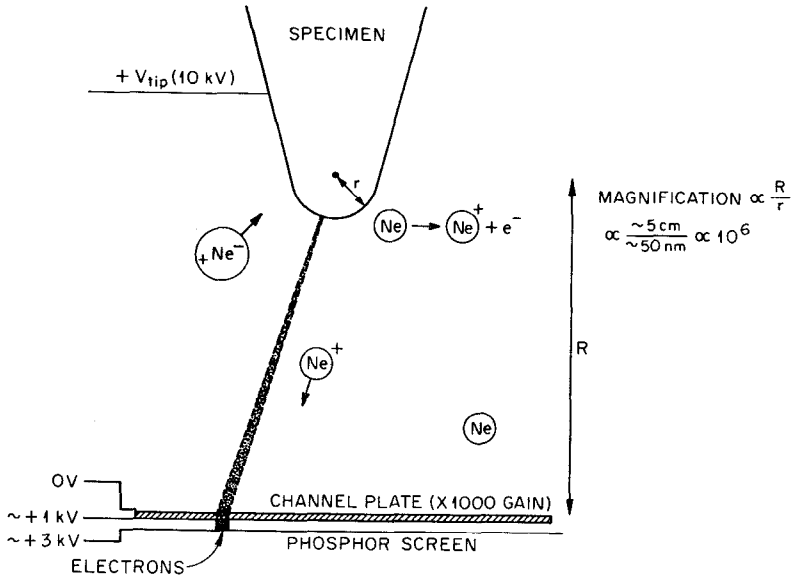

Fig. 2. Schematic diagram of a field ion microscope and the ionization process. The field ion microscope consists of a cryogenically cooled needle-shaped specimen positioned approximately 50 mm from a channel plate and phosphor screen assembly. A field ion image is formed by polarizing and then ionizing neon image gas atom near the apex of the specimen. These ions are radially projected from the specimen onto the channel plate and screen assembly where they form the field ion image.

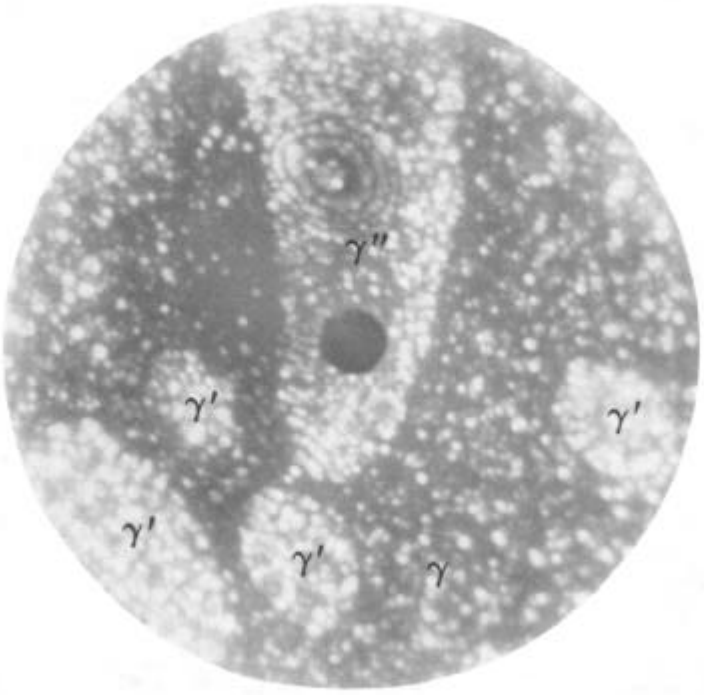

Fig. 3. Field ion micrograph of Alloy 718 after heat treatment ACDE. The brightly-imaging features are the γ'' and γ' precipitates. The central region of the dark disc in the center of the micrograph is the entrance aperture to the mass spectrometer.

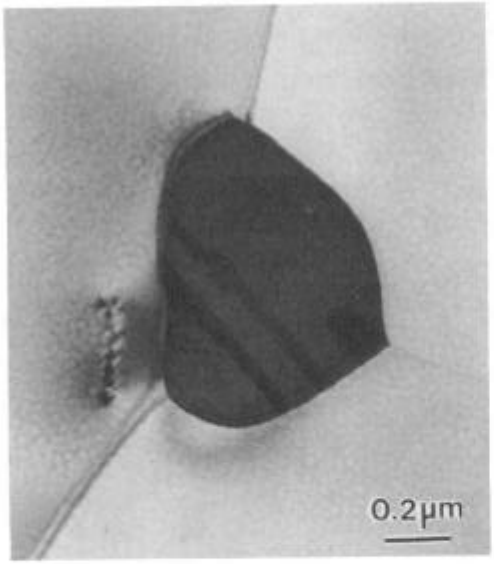

Fig. 4. TEM micrograph of a coarse Laves phase precipitate located on a grain boundary.
Heat treatment AB.

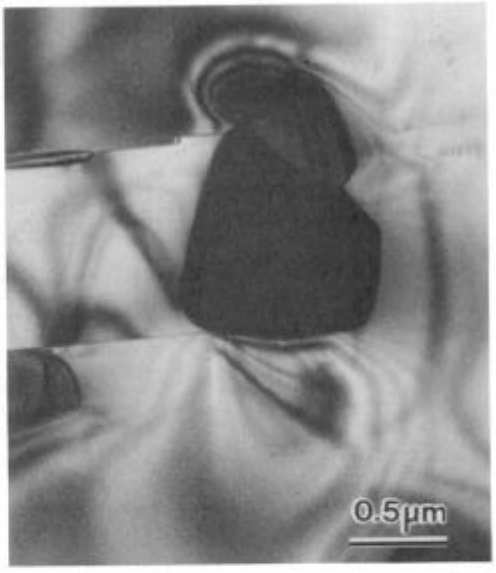

Fig. 5. TEM micrograph of a coarse MC-carbide.
Heat treatment AB.

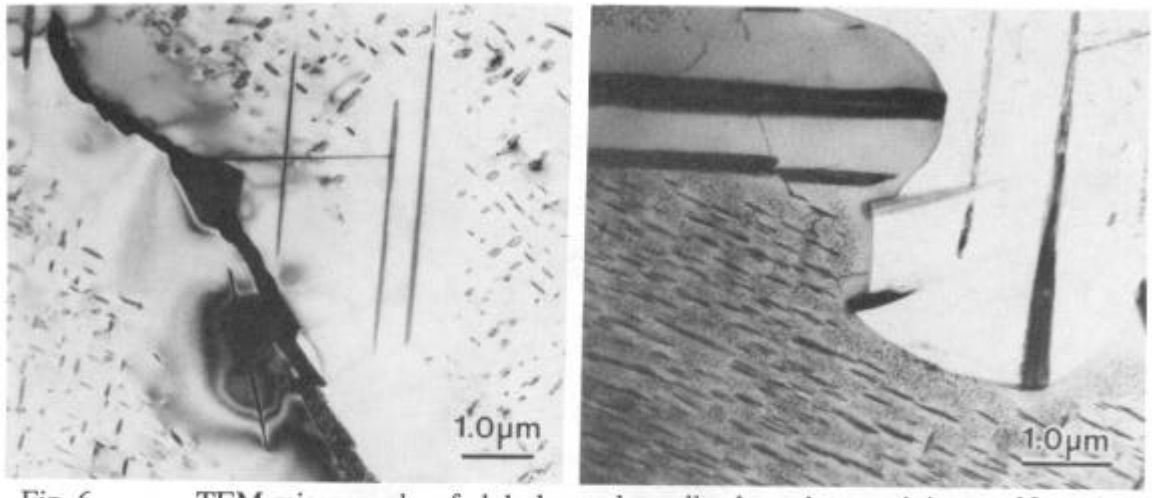

Fig. 6. TEM micrographs of globular and needle-shaped δ precipitates. Note the presence of coarse primary γ'' and a denuded zone near the δ precipitates.

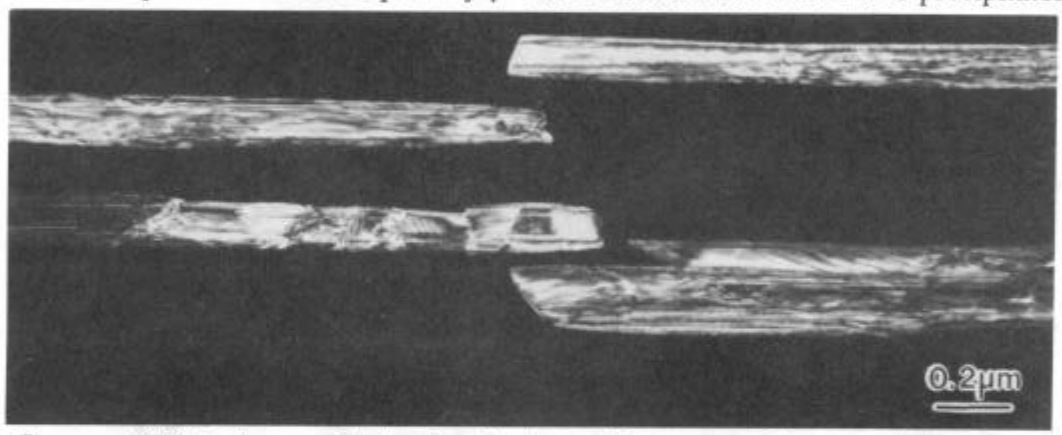

Fig. 7. TEM micrograph showing the internal structure of δ precipitates.

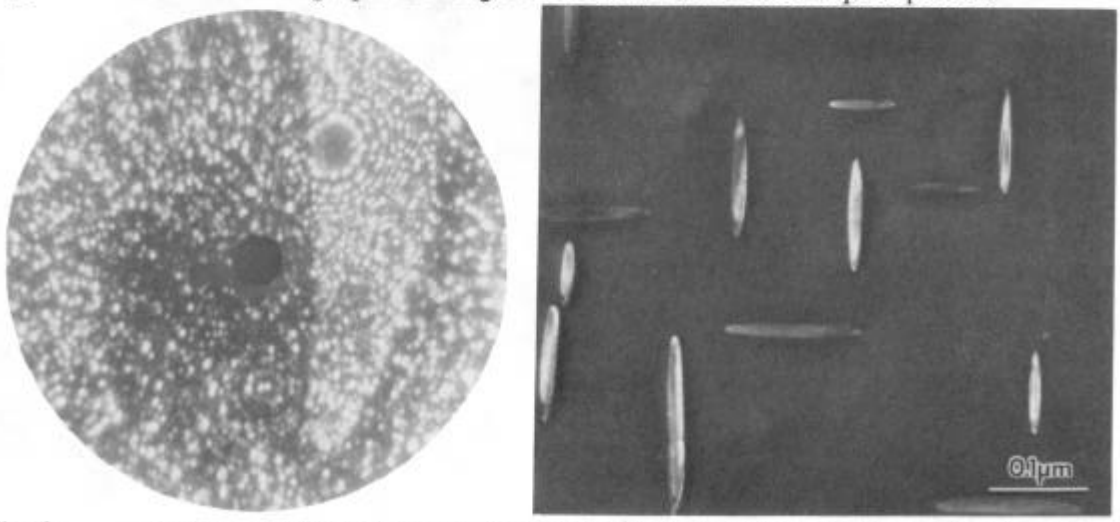

Fig. 8. FIM and TEM micrographs of primary γ'' precipitates formed after the 870°C annealing stage. Note the absence of any fine precipitates. Heat treatment AC.

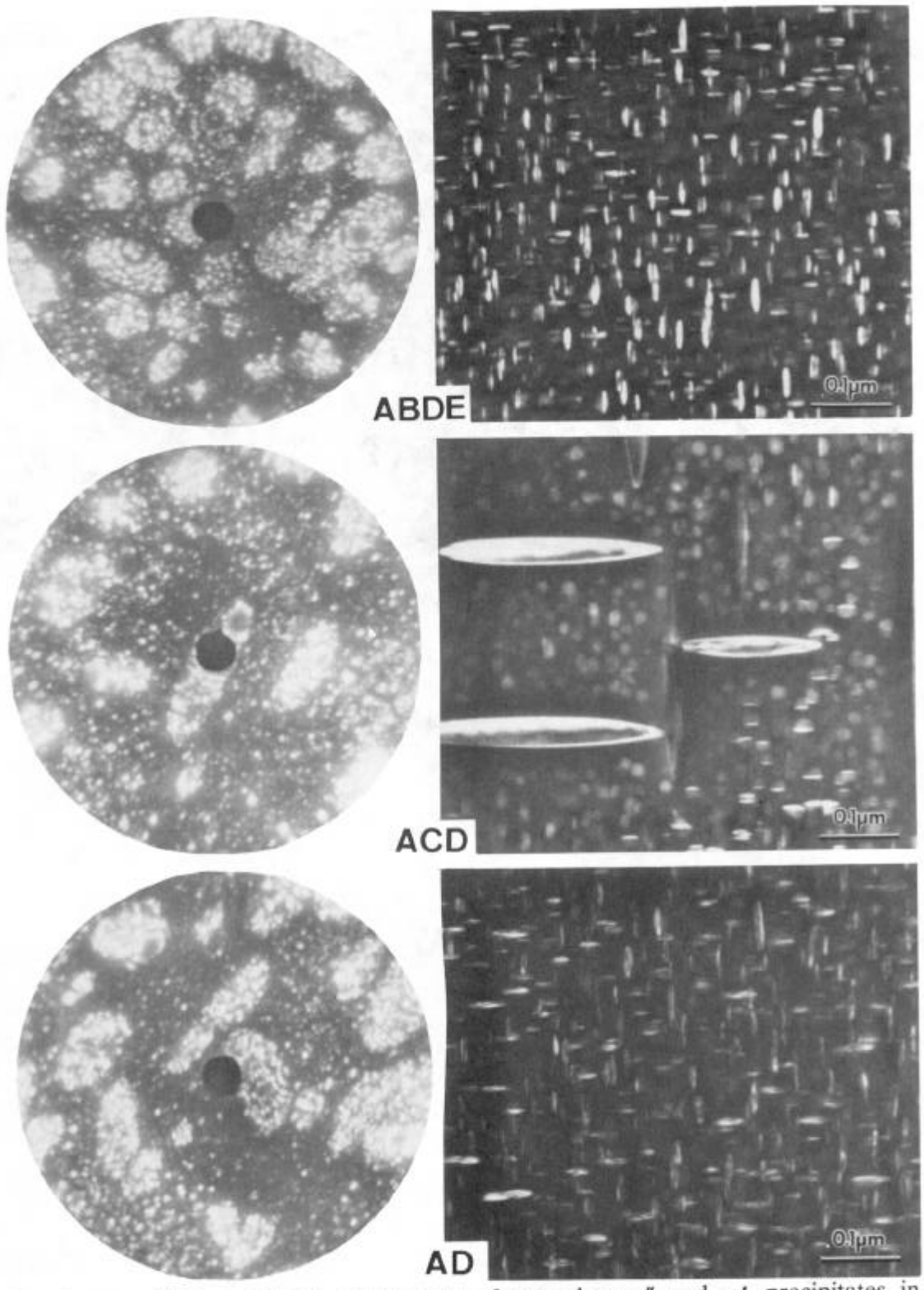

Fig. 9. FIM and TEM micrographs of secondary γ'' and γ' precipitates in materials that had been aged at 760°C. Heat treatments ABDE, ACD, and AD.

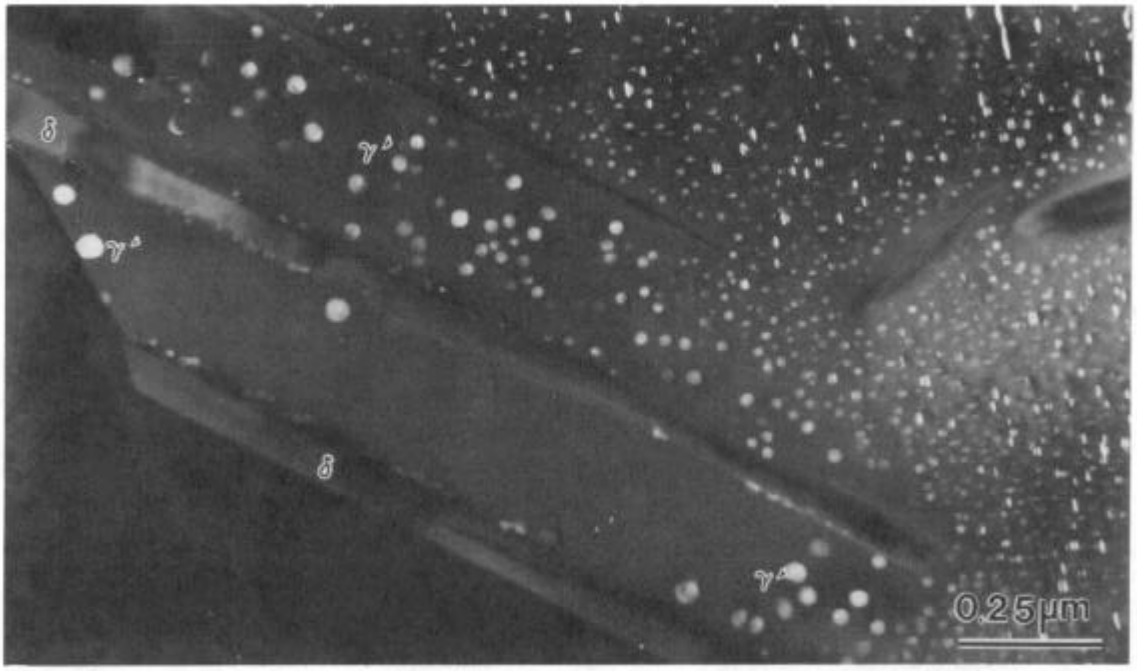

Fig. 10. TEM micrograph showing γ' precipitates in the γ'' denuded zone near a δ precipitate. Heat treatment ACD.